Structural properties of magnetic Heusler alloys

1999 J. Phys.: Condens. Matter 11 2017

(http://iopscience.iop.org/0953-8984/11/8/014)

J. Phys.: Condens. Matter **11** (1999) 2017–2026. Printed in the UK PII: S0953-8984(99)99421-3

Structural properties of magnetic Heusler alloys

A Ayuela†, J Enkovaara†, K Ullakko‡ and R M Nieminen†

† Laboratory of Physics, Helsinki University of Technology, 02015 Espoo, Finland
‡ Materials Physics Laboratory, Helsinki University of Technology, 02015 Espoo, Finland

Received 16 November 1998

Abstract. Magnetically driven actuator materials, such as the ternary and intermetallic Heusler alloys with composition X_2YM, are studied within the density-functional theory (DFT) with the generalized gradient approximation (GGA) for the electronic exchange and correlation. The geometrical and electronic structures for the magnetic $L2_1$ structure are calculated. The structures and magnetic moments at equilibrium are in good agreement with the experimental values. The structural trends with varying X and Y are explained by a d-occupation model, while a rigid-band model can account for the trends with changing M.

1. Introduction

Reversible structural deformations are interesting in view of the development of novel materials for engineering applications, for instance in robotics. Such deformations with strains up to 20% are present in the shape-memory alloys [1]. While the shape-memory effect in most of the current commercial actuator materials such as TiNi is related to a martensitic phase transformation driven by temperature, the magnetic control of such transformations would be faster and more efficient.

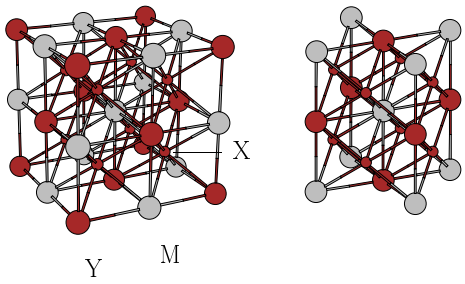

Figure 1. Unit cells of X_2YM in the cubic (left) and tetragonal (right) structures.

Some magnetically driven actuators, such as the ternary and inter-metallic Heusler alloys with composition X_2YM, are being developed. A prototypical example is Ni_2MnGa [2]. Several studies have examined the magnetic properties and structures of these alloys by means of x-ray and neutron diffraction measurements [3, 4]. They have shown that the alloys present ordered $L2_1$ structures (see figure 1), with mainly ferromagnetic ordering. In addition, some research has been done on the structural phase transformation as deformations of the $L2_1$

structure in the Ni_2MnGa ferromagnetic Heusler alloy [5–13]. Three martensites have been identified in the Ni_2MnGa alloy [10, 13].

However, few *ab initio* calculations have been carried out for these Heusler alloys. For the $L2_1$ structure, some X_2MnM compounds with X = Cu, Pd, Ni, Co and M = Al, In, Sb have been studied by Kübler *et al* [14] with the augmented-spherical-wave (ASW) formalism within the local spin-density (LSD) treatment of exchange and correlation. They showed that the Mn–Mn interaction is ferromagnetic when it is mediated by the X sublattice, as in the case of Ni- and Co-based alloys. Several non-Mn-based alloys have also been studied by other authors: Co_2Ti(Sn, Al) [15], Pd_2Ti(Al, Sn) [16], and Co_2TiAl [17]. Mohn *et al* [15] noted that a spherically symmetric potential (ASA) suppresses magnetism and outlined the need for a full-potential method in order to study these materials with a strongly aspherical electron density. Fujii *et al* [18] using the LMTO method with the LSD approximation and a muffin tin for the potential, suggested that a Jahn–Teller effect causes the lattice transformation in Ni_2MnGa and Co_2NbSn.

Very little is known about other related alloys. This paper describes some Heusler alloys based on the X_2YM stoichiometry for the $L2_1$ and distorted phases: Ni_2MnM with M = Al, Ga, Sn, and the compounds Co_2MnGa, Ni_2CoGa, and Fe_2CoGa. They are studied by means of the full-potential linearized augmented-plane-wave (FLAPW) method, using a non-local approximation for the exchange and correlation potential.

The implementation of the FLAPW method is briefly described in section 2. In section 3 we report our results for the $L2_1$ structures and their tetragonal and orthorhombic distortions, and discuss their related electronic properties. Section 4 summarizes our conclusions.

2. Computational method

The FLAPW [19] method is among the most accurate band-structure methods currently available. This method is based on the first-principles density-functional theory with the generalized gradient approximation (GGA) for exchange and correlation [20, 21] throughout. The standard local spin-density approximation (LSD) [22] is used only for testing the results for several compounds against previously published results. The muffin-tin sphere radii R used are 2.1 au for Ni and Co, 2.2 for Mn, 2.3 for Al, 2.4 for Sn and Ga. Inside the atomic spheres the charge density and the potential are expanded in crystal harmonics up to $L = 6$. The number of special k-points used in the irreducible Brillouin zone integration is 74 or 172 in the respective structures of figure 1. The density–plane-wave cut-off is $RK_{\max} = 9$, which leads to about 400 basis functions, while the potential cut-off extends up to 14, so no shape approximation to the potential is necessary. The core electrons are treated fully relativistically while the valence electrons are treated scalar relativistically.

3. Results

3.1. $L2_1$

The calculations are carried out for several lattice constants of the $L2_1$ structure in the neighbourhood of the experimental values, whenever experimental data are available. The calculated total energies as a function of the lattice constant are plotted in figure 2 for several of the alloys. The theoretical lattice constant and bulk modulus for these systems are obtained by fitting the total energies to a high-order polynomial. The calculated lattice constants and other properties related to the equilibrium structures are listed in table 1. The theoretical lattice constants are in agreement with the experimental values to within 1%. The theoretical values

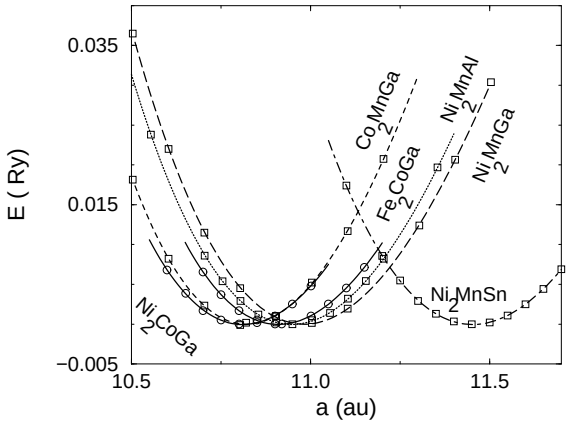

Figure 2. The total energy $\Delta E_{\rm tot}$ (relative to that of the $L2_1$ phase) of the alloys studied for different lattice constants a. Squares: Ni-based alloys; circles: others. In order from left to right: Co_2MnGa, Ni_2CoGa, Fe_2CoGa, Ni_2MnAl, Ni_2MnGa, and Ni_2MnSn.

Table 1. The theoretical lattice constant (a), bulk modulus (B), total moment ($\mu^{\rm tot}$), and spin magnetic moments (μ). Experimental values are also listed for comparison (values in brackets).

X_2YZ	a (au)	B (Mbar)	$\mu^{\rm tot}$ ($\mu_{\rm B}$)	μ^i ($\mu_{\rm B}$)
Co_2MnGa	10.82	199	4.08	0.76 (Co)
	(10.90[a])		(4.05[a])	2.72 (Mn)
				−0.07 (Ga)
Ni_2MnAl	10.95	163	4.03	0.38 (Ni)
	(11.01[a])		(4.19[c])	3.30 (Mn)
				−0.06 (Al)
Ni_2MnGa	10.98	156	4.09	0.37 (Ni)
	(11.01[a])	(146[b])	(4.17[a])	3.36 (Mn)
				−0.04 (Ga)
Ni_2MnSn	11.45	140	4.08	0.24 (Ni)
	(11.44[a])		(4.05[a])	3.53 (Mn)
				−0.03 (Sn)
Ni_2CoGa	10.81	169	1.78	0.16 (Ni)
				1.55 (Co)
				−0.02 (Ga)
Fe_2CoGa	10.92	45	6.05	2.20 (Fe)
				1.83 (Co)
				−0.07 (Ga)

[a] Reference [3].
[b] Reference [25], by means of the elastic constants.
[c] Reference [26].

are generally smaller, which may be in part due to the fact that most of the available lattice constants were measured at elevated temperatures. The theoretical saturation moments are in good agreement with the experimental ones, but are generally smaller than the measured ones, even at the experimental lattice constant. This may reflect the fact that the orbital contributions

are not included.

Our theoretical GGA values for the magnetic moments and lattice constants of $Ni_2Mn(Ga, Sn)$ are in reasonable agreement with previous self-consistent calculations [14,18]. The previous magnetic moments (distances) are 4.02, 3.75 μ_B (11.32, 11.05 au) for Ni_2MnGa and Ni_2MnSn, respectively, calculated within the local spin-density approximation. The present LSD values for the magnetic moments and for the distances of $Ni_2Mn(Ga, Sn)$ are 3.71, 3.72 μ_B and 10.67, 11.13 au. The present values are thus somewhat smaller. These differences can be explained by the assumption of a spherically symmetric potential made in previous calculations [14, 18] which decreases magnetism, and in addition gives longer distances. This is in agreement with the findings in [15]. On the other hand, the GGA full-potential values are in better agreement with the experiments than the LSD full-potential ones, which is not always the case when using spherically symmetric potentials [23]. It seems that full-potential calculations are necessary for the description of these alloys.

A more detailed description of the magnetism can give an insight into how the elements forming the material change with respect to their bulk counterparts. The magnetic moments per site are also given in table 1. The local magnetic moment of Mn is higher than in the bulk, $\mu_{\text{average}}(\text{Mn, bulk}) = 0.73\ \mu_B$ [24]. The local magnetic moment on the M site is always antiferromagnetic but with a very small value, less than 0.1 μ_B. As in the Ni-based alloys the global magnetic moment remains nearly constant, the local magnetic moment on Mn increases over X varying down or left in the Periodic Table, while as a compensation the Ni local moments decrease. This can be explained by the larger M radius which is correlated with a increase in the lattice constant and larger Mn moments as the Mn atoms are pulled apart. For the Co-based alloy, the Mn local moment is lower than in the Ni-based ones, and correspondingly the Co local moment is lower than its bulk value (1.7 μ_B). It seems that the Co is not as inactive as Ni in the Mn–Mn interaction.

The electronic state density (DOS) is given in figure 3 for the Mn-based alloys and in figure 4 for some Co-based alloys, together with a decomposition which clarifies the origin of the peak structures. The DOS in the Ni-based alloys show a similar pattern. The Fermi level E_F lies at a higher energy for the Sn alloy. These small changes are consistent with a rigid-band interpretation of the role of the M constituent, as has been previously observed [14]. The minority density of states for Co_2MnGa at the Fermi level nearly vanishes, which points to peculiar transport properties of this alloy. Changes in X can also be interpreted with a rigid band in the case of Mn alloys. The number of minority-spin states in the Co alloy decreases compared to that in the Ni alloys, as it is indicative of the changes for bulk Co and Ni metals. This is related with the small role played by the minority Mn electrons.

Larger changes observed for X and Y call for a better understanding. If we take a Y element different from Mn, as in the Co alloys (X_2CoM), the minority electrons of X and Y interact more strongly. In the case of Fe_2CoGa (see figure 4), the electronic properties follow the qualitative picture based on the fact that the minority-spin electrons in Fe lie higher in energy than those of Co. By forming bands, the Co states will have a larger weight in the low-lying bonding band, and the Fe states in the high-lying anti-bonding band, although the effect is reduced by the bonding with the non-magnetic Ga sites. A similar mechanism is also operative for Ni_2CoGa, but now mainly Co states are located below the Fermi level as can be seen in figure 4.

3.2. Structure optimization

The martensitic phase is a low-temperature phase, and its total energy at temperatures near zero should be lower than in the high-temperature phase. The shearing transformation has

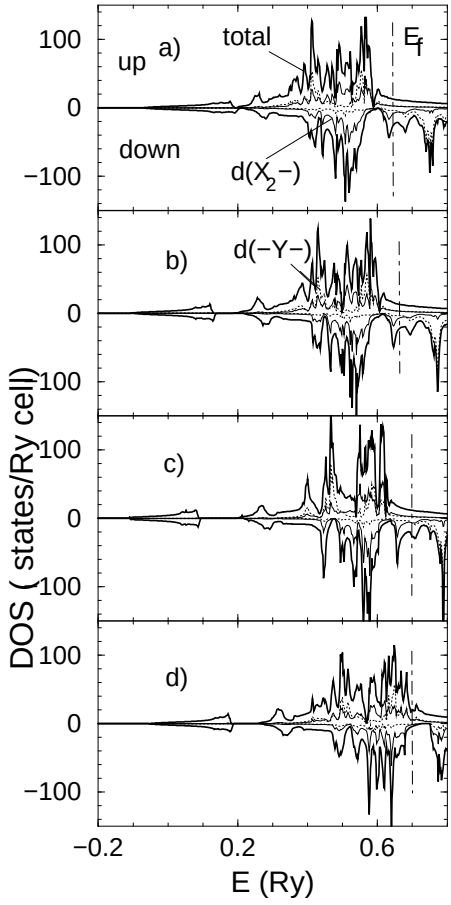

Figure 3. Total (full curve) and site-spin-projected d-electron-state densities (X_2–, full; –Y–, dotted) for ferromagnetic $XMnM_2$ alloys (a) Ni_2MnAl, (b) Ni_2MnGa, (c) Ni_2MnSn, (d) Co_2MnGa. The vertical dot–dashed line indicates the Fermi level.

been studied by making tetragonal and orthorhombic distortions to the $L2_1$ structure, keeping the volume fixed to its equilibrium value as calculated in the previous section.

3.2.1. Tetragonal distortions. The crystalline lattice of the alloys can be regarded as a body-centred-tetragonal structure which transforms through a continuous change of c/a, from the ideal $L2_1$ lattice ($c/a = 1$) to a fcc-based close-packed structure ($c/a = \sqrt{2}$). The total energy as a function of c/a is plotted in figure 5. The cubic structure is only stable in Mn alloys, except for Ni_2MnGa. In addition, there is another metastable minimum for Ni_2MnAl at $c/a = 1.22$ with a higher energy (∼0.6 mRyd per formula unit), so the temperature-driven martensitic transformation is not possible. There is an inflexion point at $c/a = 1$ for the alloys based on Co (X_2CoM). Other tetragonal minima are present at $c/a = 1.39$ and 0.86, for the compounds Ni_2CoGa and Fe_2CoGa, respectively. A rough estimate for the martensitic transformation temperature has been obtained by calculating the temperature which corresponds to the energy difference. The results—larger than 1000 K—are higher than the Curie temperatures of the respective bulk materials. As such materials should not be ferromagnetic at the transition

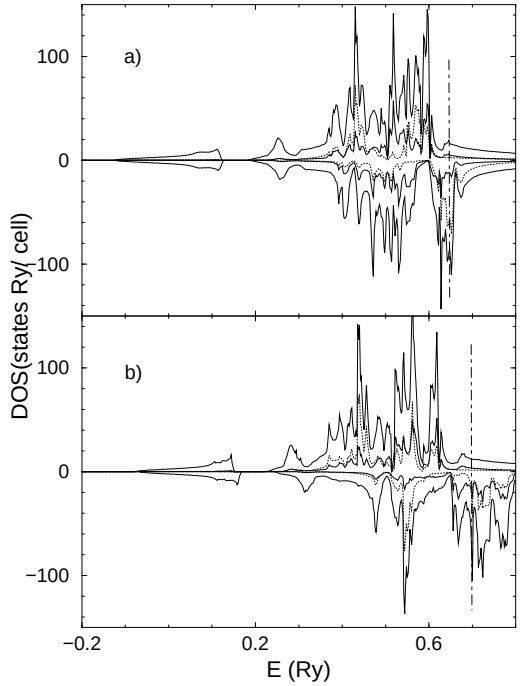

Figure 4. As figure 3, but for the Co-based alloys (a) Ni_2CoGa and (b) Fe_2CoGa.

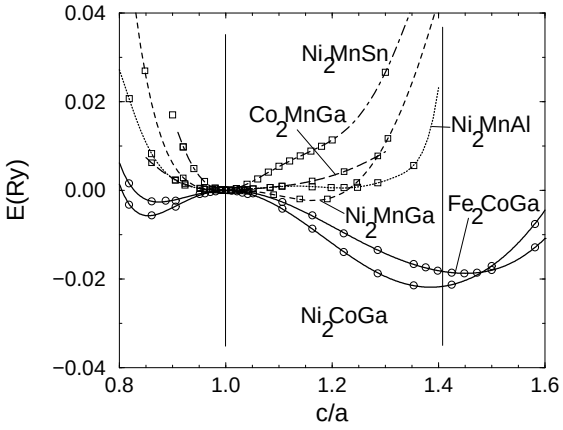

Figure 5. The total-energy difference $\Delta E_{\rm tot}^{\rm distorted}$ (relative to the $L2_1$ phase) as a function of c/a in the tetragonal distortions for the alloys: Ni_2MnAl (dotted curve); Ni_2MnGa (dashed curve); Ni_2MnSn (dotted–dashed); Co_2MnGa (long-dashed). The vertical lines at $c/a = 1$ and 1.41, respectively, represent the bct($L2_1$) and fcc-based structures (see the text).

temperature, it is not probable that they can be used as magnetically controlled actuators in the cubic phase $L2_1$.

For the Ni_2MnGa alloy the phase transformations have been experimentally studied and several modulated martensitic phases have been found [8, 9, 11]. One of them has the experimental ratio $c/a = 1.18 \pm 0.02$ which is in good agreement with the calculated value

$c/a = 1.16$. Other stable phases for $c/a < 1$ are not found, which may be for the following reasons: the shuffling of the atoms in larger and deformed cells, the constant-volume approach during the transformation, and the crystal stoichiometry. The last effect could be studied by adding some extra electrons to the primitive cell, as the rigid-band model can be used as a first approximation for the study of the electronic structure.

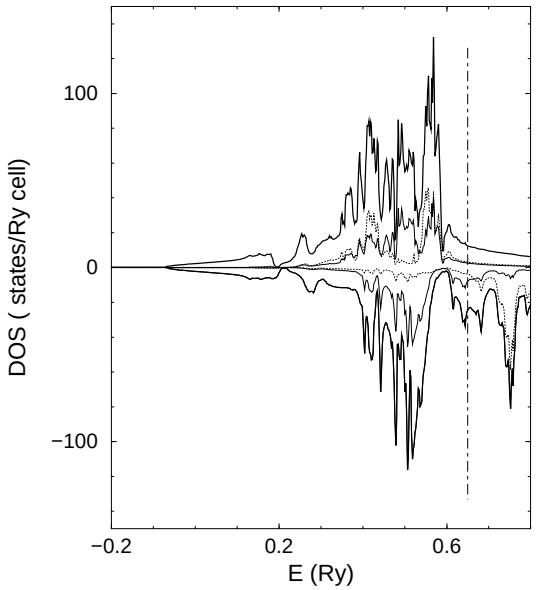

Figure 6. As figure 3(a), but with a tetragonal distortion of $c/a = 1.051$.

We now proceed to identify the physical mechanisms acting in the distortions. From the various contributions to the total energies along the tetragonal deformations, the one-electron eigenvalue sum E_{band} seems to be the key factor controlling the non-stability of the $L2_1$ structure. To understand in more detail the effects of the distortions in the band energy, the electronic density of states has been studied as a function of c/a. As an example, the density of states at $c/a = 1.051$ for Ni_2MnAl is given in figure 6 near the minimum. For $c/a \neq 1$ the minority-spin electrons just below the Fermi level are split because of the lower crystal symmetry. When $c/a > 1$, the split peaks (see figure 6) cross the Fermi level, lowering the band energy. For $c/a < 1$, the lower part of the split peak increases, so the density of states at the Fermi level diminishes, and the energy does not decrease as much as in the $c/a > 1$ case. The different behaviours in expansion and in compression can be understood through the decomposition of the different momentum components of the Al p electrons. When the lattice is compressed the Al p degeneracy is removed as in expansion, but the energy order of the peaks is reversed. As the peak crossing the Fermi level is smaller in the compression, the energy change is also smaller. The difference with respect to other Mn alloys is correlated with the location of the Fermi level as corresponding to a rigid-band model. In Ni_2MnGa the split peak is very near the Fermi level, while in Ni_2MnSn the peak does not cross the Fermi level for very small deformations because of the large number of electrons added by the Sn.

3.2.2. Orthorhombic distortions. The orthorhombic distortions are made in the $L2_1$ structure, regarded as a bct structure, by applying the axis displacements $[(1+\delta), (1-\delta), 1/(1-\delta^2)]$. The energies as a function of δ for some of the alloys studied are presented in figure 7. It can be

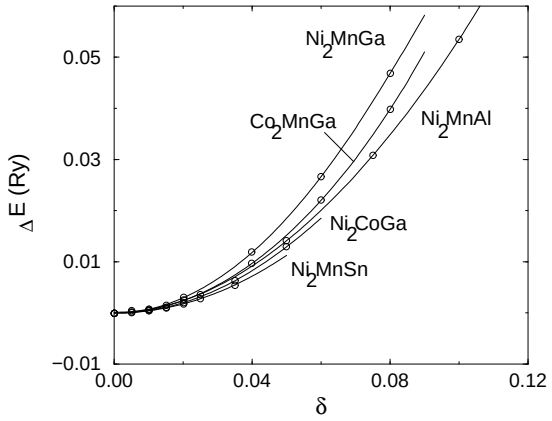

Figure 7. The total-energy difference $\Delta E_{\mathrm{tot}}^{\mathrm{distorted}}$ (relative to the $L2_1$ phase) of the alloys as a function of δ for the orthorhombic distortions (see the text for the definition of δ).

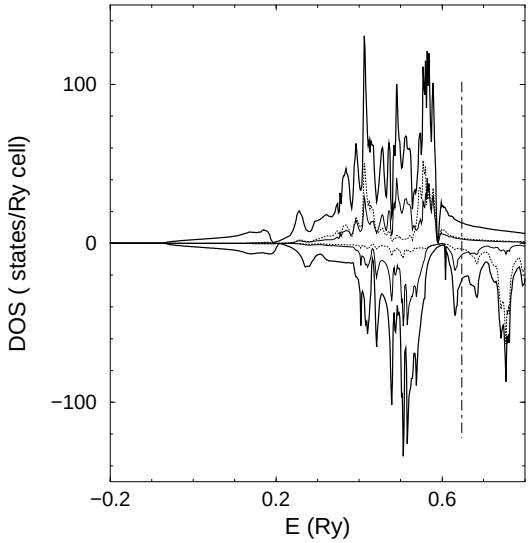

Figure 8. As figure 3(a), but with an orthorhombic distortion of $\delta = 0.025$ (see the text for the definition of δ).

seen that all of the materials are stable against these orthorhombic distortions. The density of states for Ni_2MnAl at $\delta = 0.025$ is also given in figure 8. The peak above the Fermi level has a small splitting, so the energy is not lowered. From the site DOS (see figure 8), the splitting is seen to be mainly due to the Ni d electrons.

3.2.3. Elastic constants. For some of the compounds stable against tetragonal and orthorhombic distortions, the elastic constants have been calculated. They are calculated by means of second derivatives of the energy density as $U = 6C'\delta^2$ and $U = 2C_{44}\delta^2$. The energy densities for points in the neighbourhood of $\delta = 0$, $c/a = 1$ have been fitted to (at least) fifth-order polynomials. The values of the elastic constants are presented in table 2. They compare well with the experimental elastic constants of Ni_2MnGa in the $L2_1$ structure obtained by ultrasonic

Table 2. Elastic constants for the $L2_1$ phase.

	C' (GPa)	C_{44} (GPa)	C_{44}/C'
Co_2MnGa	20	175	9
Ni_2MnAl	10	64	6
Ni_2MnSn	8	87	11
Ni_2MnGa (experimental)	22[a]	102	5
	4.5[b]	103	23

[a] Reference [25].
[b] Reference [27].

measurements, $C' = 4.5$ GPa and $C_{44} = 103$ GPa [25], $C' = 22$ GPa and $C_{44} = 102$ GPa [27].

As in a cubic crystal C_{44} and C' characterize the maximum and minimum resistance to deformation, their ratio C_{44}/C' may be used as an elastic anisotropy factor for cubic crystals ($C_{44}/C' = 1$ for an elastically isotropic material). The ratio C_{44}/C' varies between 6 and 11 for the compounds listed in table 2. The elastic anisotropy factor is highest for Ni_2MnSn. There are experimental values for Ni_2MnGa, which give values for C_{44}/C' between 5 and 23 [25, 27]. The discrepancy seems to be due to differences in the crystal stoichiometry. It affects mainly C', as has been noticed before when commenting on the influence of different alloyings through a rigid-band model.

4. Summary

The Heusler alloys $XMnM_2$ and $XCoM_2$ have been suggested as candidates for magnetically controlled shape-memory alloys (MSMA), because of their similarity to the known MSMA Ni_2MnGa. A number of alloys have been studied here by means of the FLAPW method. The equilibrium lattice constants are in good agreement with experimental data, as are the calculated magnetic moments. The possibility of martensitic transformations was studied by making tetragonal and orthorhombic distortions to the cubic $L2_1$ structure with the volume fixed to the equilibrium value. For stable $L2_1$, the three independent elastic constants of the cubic structure were also calculated on the basis of the results on the total energies of the distortions.

The alloys based on Mn can be explained with the rigid-band model, i.e. the effect of changing Y to M is to shift the Fermi level. When lowering the symmetry by tetragonal distortions, some degeneracy of the electronic energy levels is removed, and some peaks in the density of states near the Fermi level are split. In Ni_2MnGa and Ni_2MnAl alloys, the splitting already crosses the Fermi level with relatively small deformations. Thus these alloys are likely candidates for martensitic transformations. On the other hand, the Co case X_2CoM differs from that of the Mn alloys X_2MnM, because Co contributes to the minority-spin density of electronic states in the vicinity of the Fermi level. Although the Co alloys X_2CoM exhibit a total-energy minimum for $c/a \neq 1$, the energy difference between the cubic and the tetragonal phases seems too high for any practical uses as a magnetically controlled material.

It could be possible to obtain alloys exhibiting the martensitic transformation (and possibly the magnetically controlled shape-memory effect) by alloying in a small amount of Al or Sn so that the Fermi level could be shifted closer to the degenerate energy states. Also, replacing the Y atoms entirely with some other element could produce the martensitic transformation. These topics are the subject of further studies.

Acknowledgment

A Ayuela is a Marie Curie Fellow, supported by the EU TMR programme (Contract No ERB4001GT954586).

References

[1] Wayman C M 1993 *MRS Bull.* **13** (April) 49
Wayman C M 1992 *MRS Conf. Proc*. vol 246, ed C T Liur, H Otsuka and M Wuttig (Pittsburgh, PA: Materials Research Society)
[2] Ullakko K, Huang J K, Kantner C, O'Handley R C and Kokorin V V 1996 *Appl. Phys. Lett.* **69** 1996
[3] Webster P J 1969 *Contemp. Phys.* **10** 559
[4] Webster P J and Ziebeck K R A 1973 *J. Phys. Chem. Solids.* **34** 1647
[5] Kokorin V V and Chernenko V A 1989 *Phys. Met. Metallogr.* **68** 111
[6] Kokorin V V, Chernenko V A, Cesari E, Pons J and Segui C 1996 *J. Phys.: Condens. Matter* **8** 6457
[7] Kokorin V V, Osipenko I A and Shirina T V 1989 *Phys. Met. Metallogr.* **67** 173
[8] Chernenko V A, Segui C, Cesari E, Pons J and Kokorin V V 1998 *Phys. Rev.* B **57** 2659
[9] Chernenko V A, Cesari E, Kokorin V V and Vitenko I N 1995 *Scr. Metall. Mater.* **33** 1239
[10] Martynov V V 1995 *J. Physique* IV **5** C8 91
[11] Martynov V V and Kokorin V V 1992 *J. Physique* III **2** 739
[12] Ooiwa K, Endo K and Shinogi A 1992 *J. Magn. Magn. Mater.* **104–107** 2011
[13] Webster P J, Ziebeck K R A, Town S L and Peak M S 1984 *Phil. Mag.* **49** 295
[14] Kübler J, Williams A R and Sommers C B 1983 *Phys. Rev.* B **28** 1745
[15] Mohn P, Blaha P and Schwarz K 1995 *J. Magn. Magn. Mater.* **140–144** 183
[16] Jezierski A 1995 *Phys. Status Solidi* b **190** 471
[17] Guo G Y, Botton C A and Nishino Y 1998 *J. Phys.: Condens. Matter* **10** L119
[18] Fujii S, Ishida S and Asano S 1989 *J. Phys. Soc. Japan* **58** 3657
[19] Blaha P, Schwarz K and Luitz J 1997 *WIEN97* Vienna University of Technology
This is an improved and updated Unix version of the copyrighted WIEN code:
Blaha P, Schwarz K, Sorantin P and Trickey S B 1990 *Comput. Phys. Commun.* **59** 399
[20] Perdew J P and Wang Y 1992 *Phys. Rev.* B **45** 13 244
[21] Perdew J P, Burke S and Ernwerhof M 1996 *Phys. Rev. Lett.* **77** 3865
[22] Perdew J P, Chevary J A, Vosko S H, Jackson K A, Pederson M R, Singh D J and Fiolhais C 1992 *Phys. Rev.* B **46** 6671
[23] Ahuja R, Auluck S and Johansson B 1994 *Phys. Scr.* **50** 573
[24] Oberteuffer J A, Marcus J A, Schwartz L H and Felcher G P 1970 *Phys. Rev.* B **2** 670
[25] Worgull J, Petti E and Trivisonno J 1996 *Phys. Rev.* B **54** 15 695
[26] Ziebeck K R A and Webster P J 1984 *J. Phys. F: Met. Phys.* **5** 1756
[27] Mañosa L, González-Comas A, Obradó E, Planes A, Chernenko V A, Kokorin V V and Cesari E 1997 *Phys. Rev.* B **55** 11 068